WOJCIECH SZCZEPIŃSKI
JÓZEF MIASTKOWSKI

Plastic Straining of Notched Bars with Intermediate Thickness and Small Shoulder Ratio

4/1967

WARSZAWA 1967

Do użytku wewnętrznego

Zakład Mechaniki Ośrodków Ciągłych IPPT PAN
Nakład 150 egz. Ark.wyd.1,1. Ark.druk.1,75.
Druk ukończono w lipcu 1967 r.

Warszawska Drukarnia Naukowa
Warszawa, ul.Śniadeckich 8

Zam. 595/0/67.

PLASTIC STRAINING OF NOTCHED BARS WITH INTERMEDIATE THICKNESS AND SMALL SHOULDER RATIO

W. Szczepiński and J. Miastkowski
Polish Academy of Sciences, Warsaw, Poland

1. Introduction

The problem of the stress distribution and mode of deformation of notched bars undergoing tension is rather well elaborated for plane strain and plane stress conditions only. For bars with intermediate thickness, in which the truly three-dimensional state of stresses occurs, there arise such difficulties in the theoretical analysis that only the kinematical approach giving the upper bound on the load factor is available.

If the bar is sufficiently thick the plane strain complete solution is available, provided the shoulder ratio c/h is so large, that the boundary of the extended slip line field lies entirely within the contour of the bar [1]. If, however, the shoulder ratio is to small the complete solution is still not known and only the upper and lower bounds on the load factor may be obtained.

The problem on how thick a bar must be before a plane strain solution is appropriate for a V-nothed bar was experimentally investiga-

ted by W.S. Zhukovsky [2,3] and W.N. Findley and D.C. Drucker [4]. The same problem for various rounded notches was studied in authors previous paper [5]. All experimental results demonstrate that the limit load computed for perfectly plastic material has real significance for ductile metals. The experiments bring out clearly that the plane strain in a notched specimen requires the thickness b of the bar to be several times larger than the width h in the narrowest cross-section. It was found, however, that the required $\lambda = b/h$ ratio depends notably on the shape of the noth.

In the present paper upper bounds on the load factors for notched bars with intermediate thickness and small shoulder ratio are calculated and compared with experimental results. Two types of notches are investigated, namely various rounded notches and rectangular notches. Five sets of specimens of aluminium alloys were tested. It was found that the yield point load generally coincides with its theoretical upper estimate. However, the influence of the notch geometry and the ductility of the material is clearly visible.

2. Experimental technique

A universal hydraulic testing machine with ordinary pulling grips was used in all tests. In order to avoid the possible bending in the xy-plane of specimens with large c/h ratio their fitting heads were machined in the manner shown in Fig. 1.

Deformations were measured by means of a mechanical extensometer with 0.01 mm division dial gauge and length ranging from 40 mm to 60 mm depending on the shape of the notch and dimensions of the specimen. In order to minimize the effects of possible slight deviations from symmetry, causing bending in the xz-plane, two extensometers

were applied on opposite surfaces $z = \pm b$ of the specimen as shown in Fig. 1. Elongations were calculated as the mean value of readings of both extensometers. It was found that such measuring technique assures good reproducibility of experimental results. The load-deformation curves thus obtained display regular characteristics.

Depending on the material of the bar and the shape of the notch the load-elongation diagrams displayed different behaviour. Typical curves are shown in Fig. 2. The straight initial portion OA of each curve corresponds to the fully elastic state of the bar. The slight curvature of the diagram above A is connected with the growth of the plastic zones, while the elastic central part of the narrowest cross-section assures small total elongation. Unrestricted plastic flow, which should be identified with the yield point load, begins at the plastic zones meet on the axis of symmetry. This moment is clearly visible as the point B on the curve 1. However, often the moment in which the entire cross section reaches fully plastic state is hardly visible /see curves 2 and 3/. In such cases conventional definitions of the yield point load were employed. If the fully plastic portion of the diagram has slight curvature, the most convenient definition of the yield point load is to identify it with the point B of intersection of the extrapolated smooth portion of the diagram as shown on the curve 2. If, however, the curvature is considerable, as in the case of the diagram 3, the yield point load has been identified with the point B at which the tangent modulus reaches the value $0.3 \tan\alpha$, where α is the angle which makes the initial straight portion of the diagram with the elongation axis.

3. Theoretical upper bounds on the yield point load

Let P^M denotes the unknown true value of the yield point load. An

upper bound P_u on P^* may be found by equating the work done by P to the internal dissipated energy for any kinematically admissible deformation mode, considered as plastic only [6].

The yield point load factor of the notched bar will be defined as the ratio $f = P^*/P_o$, where $P_o = 8kbh$ is the yield point load of the smooth bar with constant cross-section area 4bh. The upper bound on f is equal to

$$f_u = P_u/P_o. \qquad /3.1/$$

Fig. 3 shows four different kinematically admissible mechanisms of plastic collapse of a bar with circular notch. It is evident that these collapse modes can be also applied to the upper bound estimate of the yield point load of bars with another shapes of notches. All formulas for upper bound on f_u given in this and following sections have been calculated by assuming the Tresca yield criterion.

Mechanism I represents the slip-line solution [7] for plane strain. In plane strain conditions / $\lambda = b/h \to \infty$/ it consitutes the complete solution, provided the shoulder ratio $\varkappa = c/h$ is so large that the boundary of the extended slip-line field lies entirely within the contour of the bar. It can be, however, easily verified that all kinematic conditions do not change if the shoulder ratio $\varkappa = c/h$ is smaller than required by the theory and if the $\lambda = b/h$ ratio is finite. Thus the slip-line solution may be treated as kinematically admissible deformation mode for bars with intermediate c/h and b/h ratios, giving for such bars an upper bound estimate on the unknown true value of the yield point load.

Mechanism II [8] contains a simple shear plane shaded in Fig. 3. The upper part of the bar above this plane moves as a rigid body in the direction parallel to the shear plane, while the lower part may be assumed to be immovable. The lowest value of the upper bound on

the yield point load is obtained if the shear plane makes an angle of 45^0 with the axis of the bar. The upper bound on the load factor is independent on the $\lambda = b/h$ ratio and is equal to.

$$f_u^{II} = \frac{1 + \partial\ell}{2}, \qquad /3.2/$$

where $\partial\ell = c/h$. Formula /3.2/ is valid for all shapes of notch. It will be shown later that /3.2/ gives the best upper bound for sufficiently large λ and small $\partial\ell$.

Mechanism III [9] consists in a simple 45^0 discontinuous rigid blocks motion as shown in Fig. 3. For majority of notch shapes, among them for circular and V-shaped notches this mechanism gives the following upper bound on f

$$f_u^{III} = 1 + \frac{\sqrt{2}}{4}\lambda. \qquad /3.3/$$

If, however, the narrowest part of the notch is formed by two straight lines parallel to the axis of the bar, as for example in the case of a rectangular notch /Fig. 1/, and if 2e denotes the length of this straight bottom part of the notch, the formula for the upper bound takes the form.

$$f_u^{III} = 1 + \frac{\sqrt{2}}{4}\left(\lambda - \frac{\beta^2}{\lambda}\right), \qquad /3.4/$$

where $\beta = e/h$ is a parameter depending on the length 2e.

Mechanism IV represents simple shearing along a discontinuity plane making an angle of 45^0 with the axis of the bar. The shear plane is shaded in Fig. 3. This mechanism gives the best lower bound on the load factor for small $\lambda = b/h$. Since the shear area depends on the shape of the notch the upper bound on the load factor f_u^{IV} has to be

computed for each particular notch.

Let us consider now an important case of notched bars approaching to the plane strain conditions $\lambda \gg 1$ but having small shoulder ratio $\varkappa = c/h$. For such bars not only an upper bound on f given by mechanism II may be obtained but also a lower bound from an appropriate statically admissible stress field can be found. Lower bounds for a rounded notch and a rectangular notch may be obtained from the fields shown in Fig. 4. Let us consider a bar with rounded notch of a radius a and small shoulder width c /Fig. 4a/. We can always find such radius a^* of a circular notch for which the extended slip-line field calculated in the manner shown by Bishop [1] will lie entirely within the contour of the bar considered of radius a and shoulder width c, as shown in the figure. Thus assuming the material outside the slip-line field to be stress-free we obtain the lower bound f_1 on the load factor to be equal to the actual load factor of a bar with a notch of a radius a^*. The same technique may be applied for different shapes of notches. Fig. 4b shows a bar with rectangular notch of length 2e with inscribed slip-line field corresponding to another length $2e^*$.

4. Upper bounds for bars with a circular notch.

Let us consider now a bar with a circular notch of a radius a /Fig. 5/. The shape of the notch is characterized by the parameter $\mu = a/h$. Thus the yield point load will be determined by three independent parameters

$$0 \leq /\mu = a/h/ \leq \infty, \quad 0 \leq /\lambda = b/h/ \leq \infty, \quad 1 \leq /\varkappa = c/h/ \leq \infty.$$

Depending on the values of these parameters the best upper bound on the yield point load factor f_u will be furnished by one of the mechanisms shown in Fig. 3. For a given value of the parameter μ the best kinematically admissible collapse mode will depend upon values

of both remaining parameters $\mathcal{H}$ and λ. Fig. 5 shows in the $\mathcal{H}, \lambda$ plane regions corresponding to various collapse mechanisms for the particular value $\mu = 0.6$. Similar diagrams may be easily obtained for any arbitrary value of μ. Thus all formulas given below will be written for an arbitrary.

The region I corresponds to the slip-line mechanisms I, and in this range of $\mathcal{H}$ and λ the lowest upper bound on the load factor may be calculated from Hill's [7] formulas

$$f_u^I = \begin{cases} (1 + \mu) \ln(1 + \frac{1}{\mu}) & \text{for } \mu \geq 0.263, \\ 1 + \frac{\pi}{2} - \mu e^{\pi/2} - 1 - \frac{\pi}{2} & \text{for } \mu < 0.263. \end{cases} \qquad /4.1/$$

The upper bound on f in the region II, for which the mechanism II is appropriate, will be determined by /3.2/.

In the region III, where the mechanism III gives the lowest of the upper bound, the formula /3.3/ for f_u holds.

Much more complicated form take the formulas for f_u in the region IV corresponding to the collapse mechanism IV. This region is divided into three subregions IVa, IVb and IVc. In each of these subregions the expression for f_u takes a different form, because the shaded area in Fig. 3 cannot be described by one general expression valid in all three possible geometric configurations.

Thus in the field IVa we have

$$f_u^{IVa} = \mathcal{H}(1 - \frac{\mu}{\lambda}) + \frac{\mu}{\lambda}\left[1 + \mu(1 - \frac{\pi}{4})\right]. \qquad /4.2/$$

The field IVb corresponds to the following upper bound

$$f_u^{IVb} = \mathcal{H} - \frac{1}{2\lambda}\left[\frac{\pi\mu^2}{2} - \mu^2 \arccos\frac{1}{\mu}\sqrt{(2\mu + 1 - \mathcal{H})(\mathcal{H} - 1)}\right. -$$

$$- /1 + \mu - \varkappa/\sqrt{/2\mu + 1 - \varkappa//\varkappa - 1/}\,]. \qquad /4.3/$$

In the field IVc we obtain

$$f_u^{IVc} = 1 + \mu - \frac{1}{2}\sqrt{\mu^2 - \lambda^2} - \frac{\mu^2}{2} \arccos \frac{\sqrt{\mu^2 - \lambda^2}}{\mu}. \qquad /4.4/$$

The equations of the lines separating all six regions in Fig. 5 are as follows

line	equation in the $\varkappa$, λ coordinates / μ is a parameter/	
AB	$\varkappa = 2\,/1 + \mu/\,\ln/1 + \frac{1}{\mu}/ - 1$	for $\mu \geqslant 0.263$
	$\varkappa = 2\,/1 + \frac{\pi}{2} - \mu/e^{\pi/2} - 1 - \frac{\pi}{2}/ - 1$	for $\mu < 0.263$
BC	$\lambda = \frac{4}{\sqrt{2}}\left[/1 + \mu/\,\ln/1 + \frac{1}{\mu}/ - 1\right]$	for $\mu \geqslant 0.263$
	$\lambda = \frac{4}{\sqrt{2}}\left[\frac{\pi}{2} - \mu/e^{\pi/2} - 1 - \frac{\pi}{2}/\right]$	for $\mu < 0.263$
BD	$\varkappa = 1 + \frac{\sqrt{2}}{2}\lambda$	
DG	$\varkappa = \dfrac{\lambda + \frac{\sqrt{2}}{4}\lambda^2 - \mu\left[1 + \mu/1 - \frac{\pi}{4}/\right]}{\lambda - \mu}$	
DE	$\varkappa = \dfrac{\lambda - 2\mu\left[1 + \mu/1 - \frac{\pi}{4}/\right]}{\lambda - 2\mu}$	
EF	$\varkappa = 1 + \mu$	
FH	$\lambda = \mu$	
EK	$\lambda = \frac{1}{\varkappa - 1}\left\{\frac{\pi\mu^2}{2} - \mu^2 \arccos \frac{1}{\mu}\sqrt{/2\mu + 1 - \varkappa//\varkappa - 1/} - \right.$ $\left. - /1 + \mu - \varkappa/\sqrt{/2\mu + 1 - \varkappa//\varkappa - 1/}\right\}$	
FK	$\varkappa = 1 + \mu - \sqrt{\mu^2 - \lambda^2}$	

5. Upper bounds for bars with a rectangular notch

The analysis for bars with a rectangular notch /Fig. 6/ is much simpler than in the previous case. The shape of the notch is characterized by the parameter $\beta = e/h$. The yield point load depends upon three independent parameters

$$0 \leq /\beta = e/h/ \leq 1, \quad 0 \leq /\lambda = b/h/ \leq \infty, \quad 1 \leq /\mathfrak{a} = c/h/ \leq \infty.$$

Fig. 6 shows in the $\mathfrak{a}$, λ plane the regions in which particular mechanisms of plastic collapse from Fig. 3 give the lowest estimate on the yield point load factor. Each region is marked by a number corresponding to the number of the respective mechanism. Fig. 6 is drawn for a particular value of the parameter $\beta = 0.24$. For other values of β the general picture of the diagram does not change, the only difference being in the change of positions of the points B and D. The trajectory of the point B is marked by dashed line. Small circles show the positions of B for various values of β. Point D moves along the λ-axis, its ordinate being $\lambda = \beta$.

In the field I the best upper bound is connected with the slip-line mechanism. In the contrary to the previously discussed case of a circular notch, the value of the upper bound cannot be now expressed in closed form, since the plane strain solution can be obtained only numerically. Diagram in Fig. 7 represents the yield point load factor $\varphi/\beta/$ obtained from the plane strain solution for different values of the parameter β. Thus the value of the upper bound in the region I is constant for a fixed

$$f_u^I = \varphi/\beta/, \qquad /5.1/$$

and may be obtained from Fig. 7.

The upper bound on f in the field II, corresponding to the collapse mode II, is determined by /3.2/.

In the field III, where the mechanism III is appropriate, the best upper bound can be calculated from /3.4/.

In the field IV, in which $\lambda < \beta$, or in other words $e > b$, the mechanism IV gives obviously $f_u^{IV} = 1$.

The lines separating regions in Fig. 6 have the following equations in the $\varkappa, \lambda$ coordinates

line AB $\quad \varkappa = 2\varphi/\beta/ - 1,$

line BC $\quad \sqrt{2}/\lambda - \beta/^2 - 4\lambda[\varphi(\beta) - 1] = 0,$

line BD $\quad \varkappa = 1 + \frac{\sqrt{2}}{2}\frac{/\lambda - \beta/^2}{\lambda},$

line DE $\quad \lambda = \beta.$

6. Experimental results for bars with circular notch

Two sets of specimens with circular notch were tested. In each set the μ-parameter describing the shape of the notch had a constant value. The parameter $\lambda = b/h$ was also constant in each set. The only parameter varying in a particular set of specimens was the shoulder ratio $\varkappa = c/h$.

Although the theoretical upper bound analysis presented above refers only to the yield point load, in the present experiments not only the yield point loads but also the ultimate loads were recorded, because they can furnish valuable informations of great practical importance.

Fig. 8 shows some of the initial portions of the nominal stress versus elongations in 40 mm diagrams for the first series of specimens with a circular notch. The shape-parameter was equal $\mu = 0.6$ and the thickness-parameter was $\lambda = 2$. The material was the PA-1 aluminium alloy /according to polish standarts/, containing 1.0 ÷ 1.6 % of manganese. Arrows indicate the average yield point stresses

in the minimum section of the bar*.

The relation between the observed yield point average stress and the ratio $\varkappa$ is shown in Fig. 9 together with the theoretical curves. The upper bound curve was obtained according to the solution presented in Fig. 5. It is readily seen that for $\lambda = 2$ the best upper bound on f for bars with $\varkappa \leq 2.139$ is given by the collapse mechanism II and formula /3.2/. For $\varkappa > 2.139$ the slip-line mechanism I is appropriate. For chosen value $\mu = 0.6$ the formula /4.1/ leads to $f_u = 1.570$ in this range. Since both mechanisms I and II are valid also in the plane strain conditions it seems to be interesting to compare experimental results with the lower bound on f obtained for the plane strain conditions in the manner shown in Fig. 4a. For $\varkappa = 2.62$ the lower and upper bounds for plane strain coincide.

The experimental curve in Fig. 9 shows that the actual yield point loads are alightly greater than the theoretical upper bounds calculated for Tresca yield criterion. The ultimate nominal stress P_{max}/F_o, where F_o is the area of the narrowest cross-section of the bar, displays also considerable increase with increasing value of the $\varkappa = c/h$ ratio. It is interesting to note that for $\varkappa > 2.62$ the ultimate stress has almost constant value. The ratio of ultimate stresses for bars with $\varkappa = 6$ and $\varkappa = 1$ /unnotched bar/ is equal to 1.37, while the analogous theoretical value for yield point loads is $f = 1.57$.

In the second series of specimens with circular notch all dimensions were the same as in the first set except the thickness $2b = 10$ mm. Thus the thickness-width ratio was equal to $\lambda = b/h = 1$. The material was the PA-2 /2.0 ÷ 2.8 % Mg, 0.2 ÷ 0.4 % Mn/ aluminium alloy.

Fig. 10 shows the initial portions of the nominal stress versus elongation in 40 mm diagrams. The yield point loads were obtained in the manner shown in Fig. 3 - curve 3. The relation between thus obtained yield point nominal stress P_{pl}/F_o and the shoulder ratio $\varkappa = c/h$

* All dimensions in figures are given in milimeters.

is shown in Fig. 11. According to Fig. 5 the theoretical upper bounds on f for bars with $\lambda = 1$ and $\alpha \leq 1.707$ will be defined by the collapse mechanism II and formula /3.2/ as in the previous case. For $\alpha > 1.707$, however, the collapse mechanism III and formula /3.3/ are appropriate, from which the value $f_u = 1.354$ was calculated. The theoretical upper bounds are shown in Fig. 11 by dashed lines. As in the previous case the actual yield point stresses are slightly greater than their theoretical upper estimates. The ultimate nominal stress P_{max}/F_o curve displays similar behaviour as the yield point stress P_{pl}/F_o curve. For $\alpha > 2$ the ultimate stress has almost constant value, which is approximately 1.18 times larger than the ultimate stress for an unnotched bar /$\alpha = 1$/.

7. Experimental results for bars with rectangular notch

Three sets of rectagularly notched specimens were tested. The $\beta = e/h$ - parameter describing the shape of the notch was the same for all specimens belonging to one set. Each set of specimens was, however, characterized by another value of β. The parameter $\lambda = b/h$ was also constant in each set. The only parameter varying in a particular set of specimens was the shoulder ratio $\alpha = c/h$.

In the first set all specimens were characterized by the parameters $\lambda = 2.00$ and $\beta = 0.12$. The material was PA-1 aluminium alloy. Fig. 12 shows initial portions of some nominal stress - elongation on the base 40 mm diagrams. The method by means of which the conventional yield point stresses were obtained is shown on each curve. The best upper bound for $\alpha \leq 2.25$ can be obtained from the mechanism II. For $\alpha > 2.25$ the upper bound connected with the mechanism III /see Fig. 6/ is constant and has the value $f_u = 1.64$. Theoretical upper bounds on yield point stresses calculated for various α are repre-

sented by dashed line in Fig. 13. The experimental yield point stresses P_{pl}/F_o are slightly greater than their theoretical upper estimates. The ultimate average stresses P_{max}/F_o also display considerable increase with increasing $\varkappa$ for small values of $\varkappa$ and reach practically constant value for $\varkappa \geq 3$, the ratio of this maximum value to the ultimate stress for an unnotched bar /$\varkappa = 1$/ being 1.42.

The material used in the two last sets of specimens was the duraluminium PA-6, having much worse ductility than materials used in the tests.

Fig. 14 shows initial portions of the nominal stress - elongation diagrams for some specimens characterized by $\beta = 0.08$ and $\lambda = 2.50$ and various values of $\varkappa$. The experimental P_{pl}/F_o curve lies below the theoretical upper estimates on the yield point load shown by the dashed line in Fig. 15. Since three specimens were machined from another stock of the material, the experimental results for them are marked by triangles. For $\varkappa > 2.65$ the upper bound on the yield point load factor given by the collapse mechanism III is equal to $f_u = 1.85$, whille the experimental value calculated for $\varkappa = 9.6$ is much smaller and equals only 1.54. The ultimate nominal stresses P_{max}/F_o for large $\varkappa$ are only 20 % larger than ultimate stresses for the smooth bar /$\varkappa = 1$/.

In the last series of specimens the parameters $\beta = 0.24$ and $\lambda = 5.00$ have been choosen. The yield point stresses obtained from the nominal stress - elongation diagrams /Fig. 16/ are also this case smaller than their theoretical upper estimates shown in Fig. 17 by the dashed line. For $\varkappa = 9.6$ the actual yield point stresses are 1.65 times larger than analogous stresses for $\varkappa = 1$, while the corresponding theoretical ratio obtained using the upper bound technique is equal to 1.83. The ratio of ultimate nominal stresses P_{max}/F_o for bars with $\varkappa = 9.6$ and $\varkappa = 1.0$ has the value 1.38.

8. Concluding remarks

Experimental results demonstrate that the agreement between the theoretical upper estimates of the yield point loads and their values is quite satisfactory for aluminium alloys displaying good ductility. For less ductile materials PA-6 /duraluminium as received/ the actual yield point load is remarkably smaller than the theoretical estimate. The difference between theoretical and experimental results for PA-6 alloy depends on the shape of the notch, being approximately 10 % for $\beta = 0.24$ and 17 % for $\beta = 0.08$.

It is interesting to note that the ultimate nominal stresses P_{max}/F_0 increase with increasing $\partial\ell$, until at a certain $\partial\ell$ reach their maximum value. For still larger $\partial\ell$ the ultimate stresses do not change. The ratio of this maximum value of the ultimate stresses and the ultimate stresses for a smooth bar $/\partial\ell = 1/$ is for all tested materials and shapes of the notch much smaller than the analogous ratio for yield point nominal stresses. The less ductile is the material and the sharpest is the notch the greater is the difference between both ratios.

References

1. J.F.W. Bishop, On the complete solution to problems of deformation of a plastic-rigid material, J. Mech. Phys. Solids, vol. 2, 1953, pp. 43 - 53.
2. W.S. Zhukovsky, Deformations and stresses in plane notched bars, /in Russian/, Problems of Strength in Machine Design - ser. 2, Academy of Sciences USSR, Moscow 1959.
3. W.S. Zhukovsky,,Strength of plane notched bars with arbitrary thickness, /in Russian/, Strength Analisis - ser. 9, Mashgiz,

Moscow 1963, pp. 231 - 252.

4. W.N. Findley, D.C. Drucker, An experimental study of plane plastic straining of notched bars, J. Appl. Mech., vol. 32, 1965, pp. 493--503.
5. W. Szczepiński, J. Miastkowski, Experimental analysis of plastic yielding of notched bars, /in Polish/, Rozprawy Inżynierskie vol. 13, 1965, pp. 637 - 652.
6. D.C. Drucker, H.J. Greenberg and W. Prager, Extended limit design theorems for continous media, Q. Appl. Math. vol. 9, 1952, pp. 215 - 389.
7. R. Hill, The plastic yielding of notched bars under tension, Quart. J. Mech. Appl. Math. vol. 2, 1949, p. 40.
8. W. Prager, P.G. Hodge, Theory of Perfectly Plastic Solids, J. Wiley Inc., 1951, pp. 215 - 216.
9. D.C. Drucker, On obtaining plane strain or plane stress conditions in plasticity, Proc. 2nd U.S. Nat. Congr. Appl. Mech.- 1954, pp. 485 - 488.

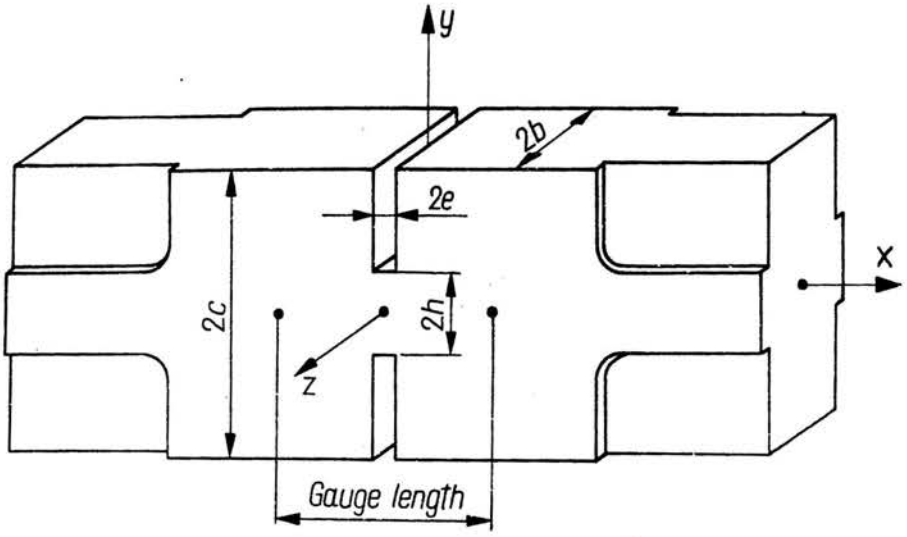

Fig.1

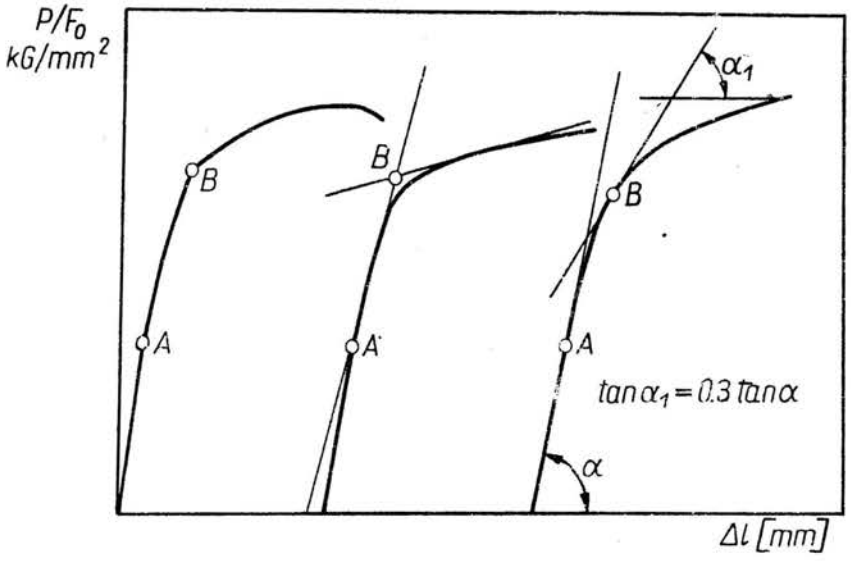

Fig. 2

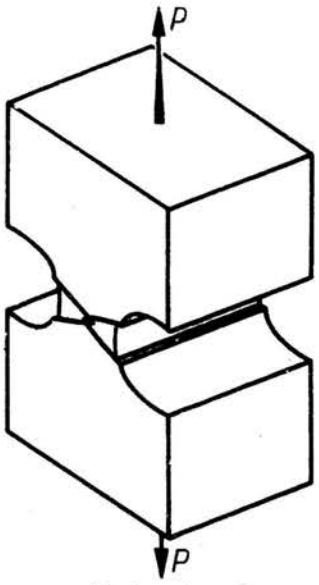

Mechanism I

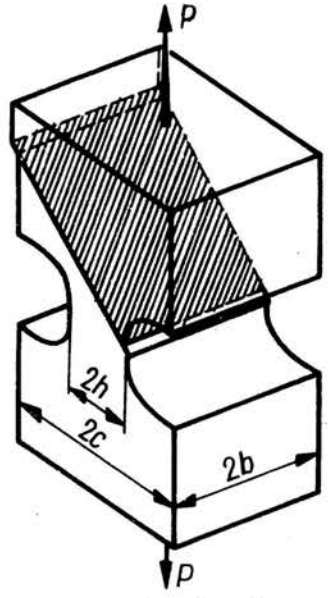

Mechanism II

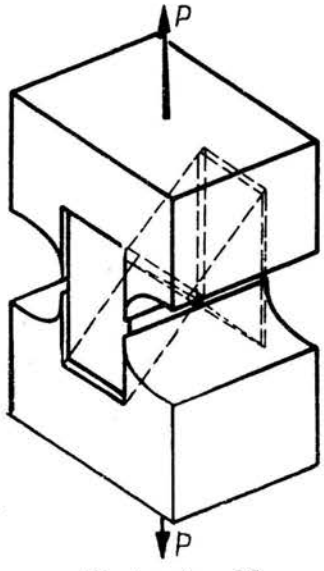

Mechanism III

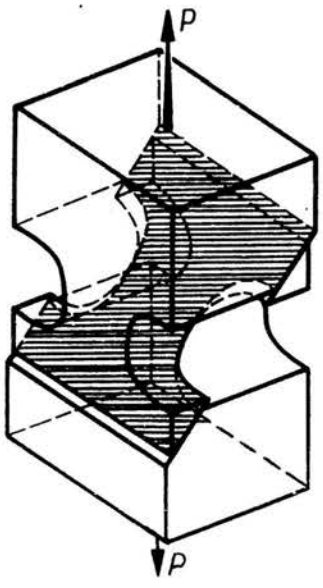

Mechanism IV

Fig. 3

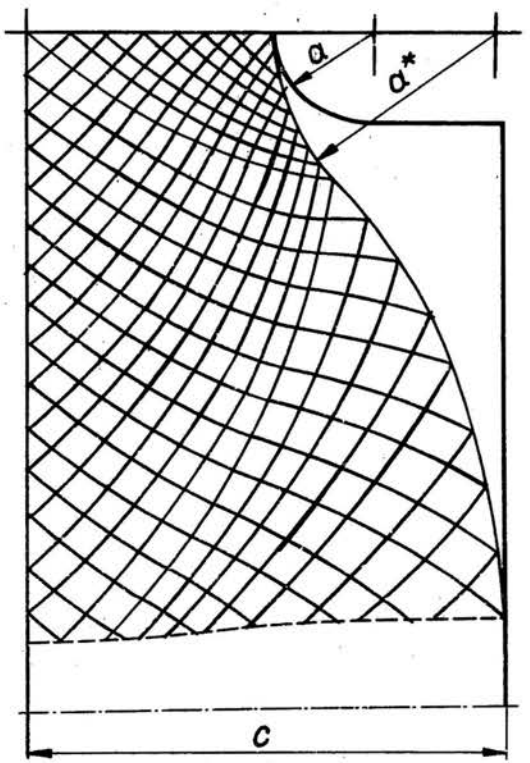

Fig. 4a

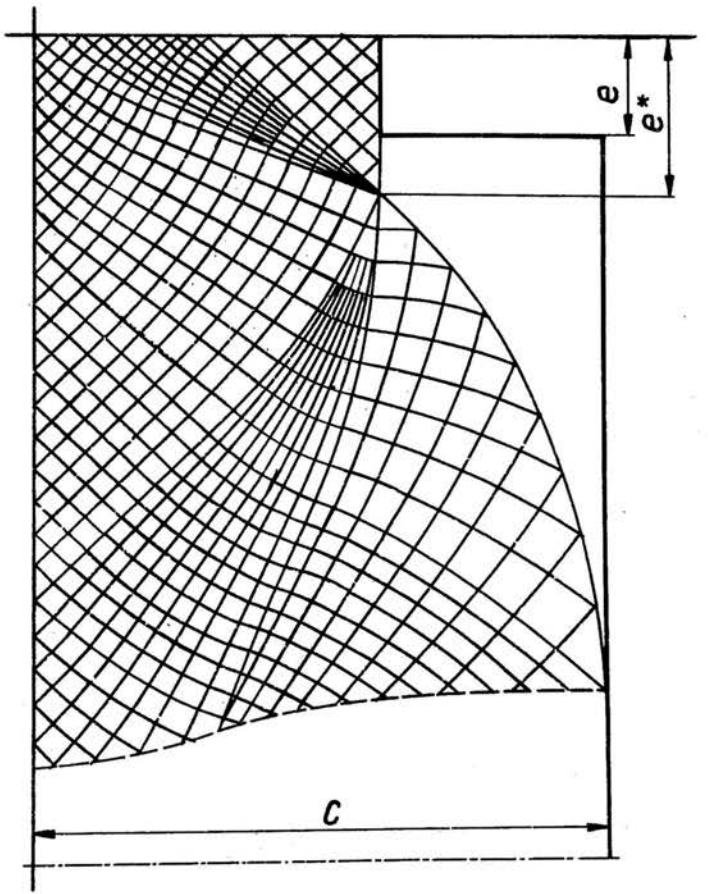

Fig. 4b

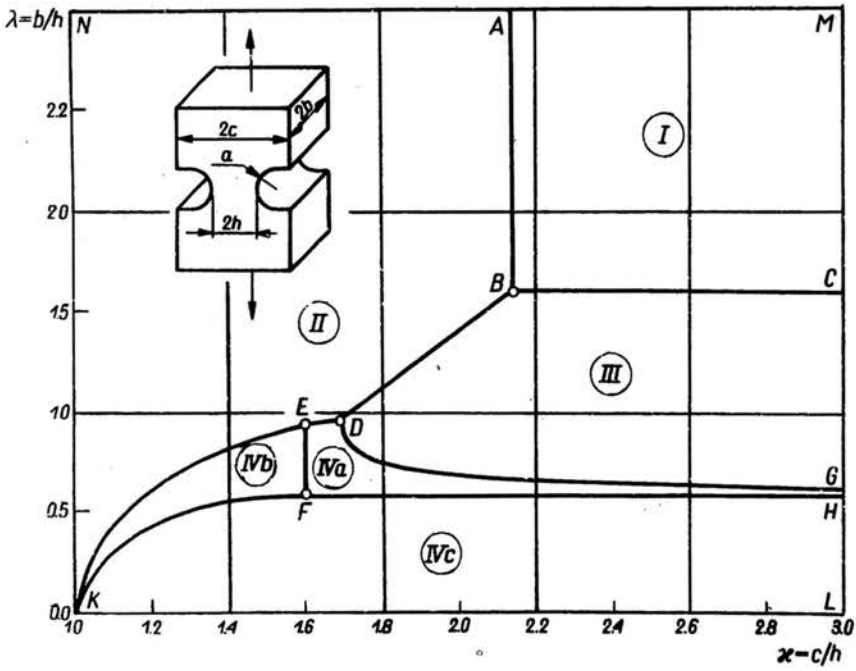

Fig. 5

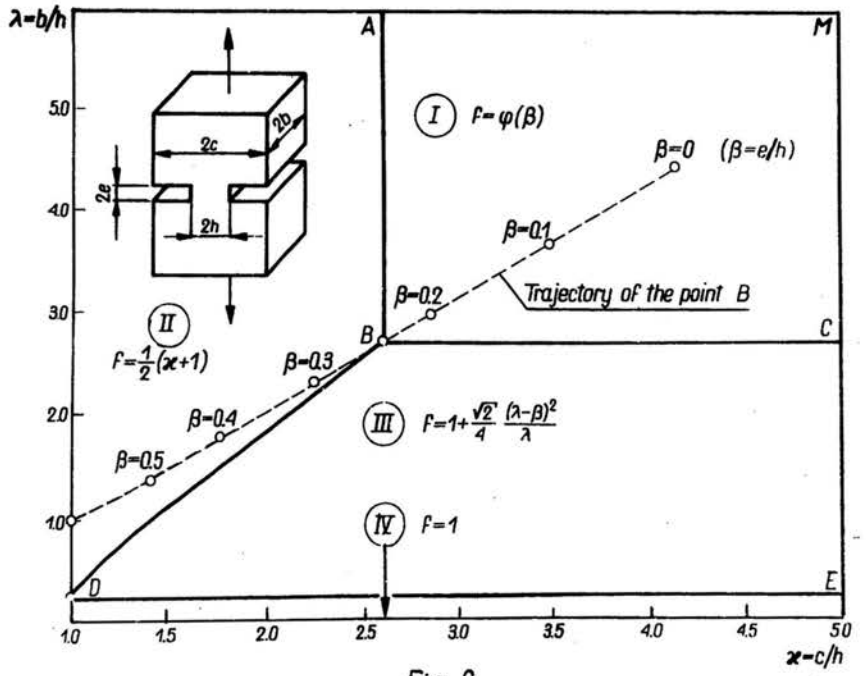

Fig. 6

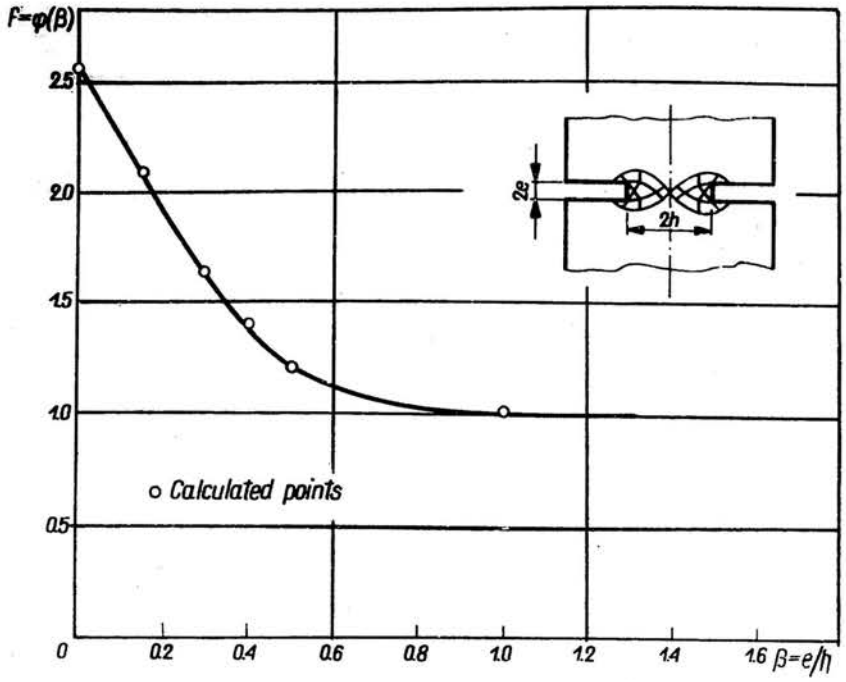

Fig. 7

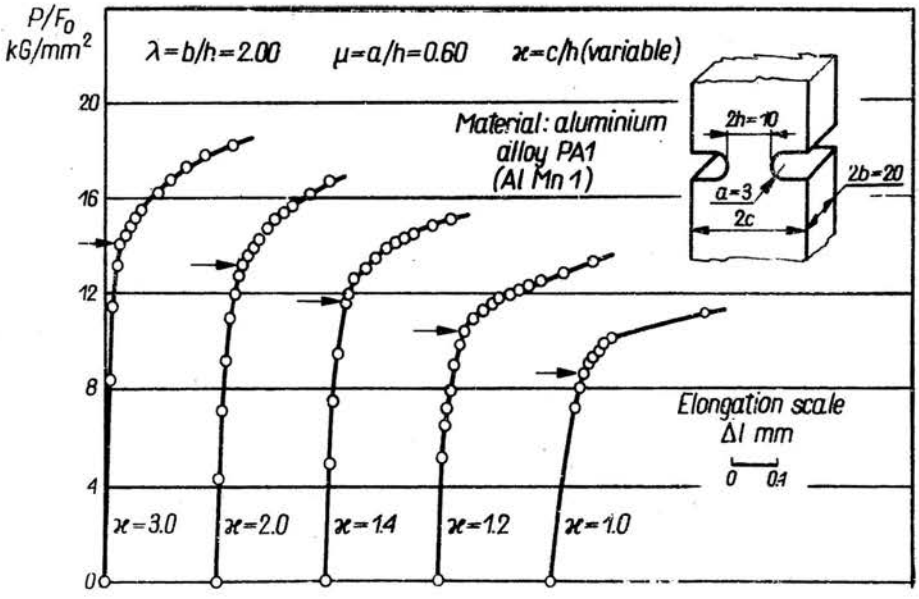

Fig. 8

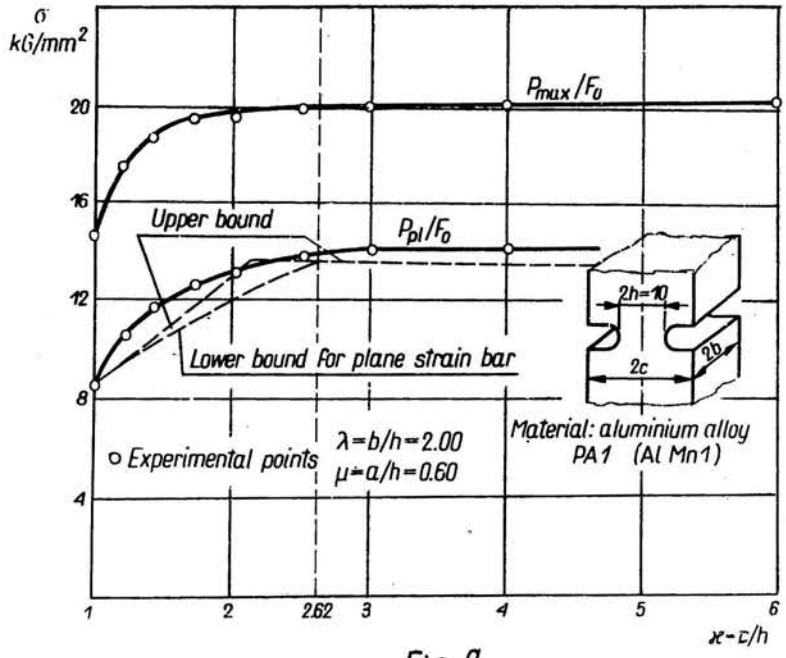

Fig. 9

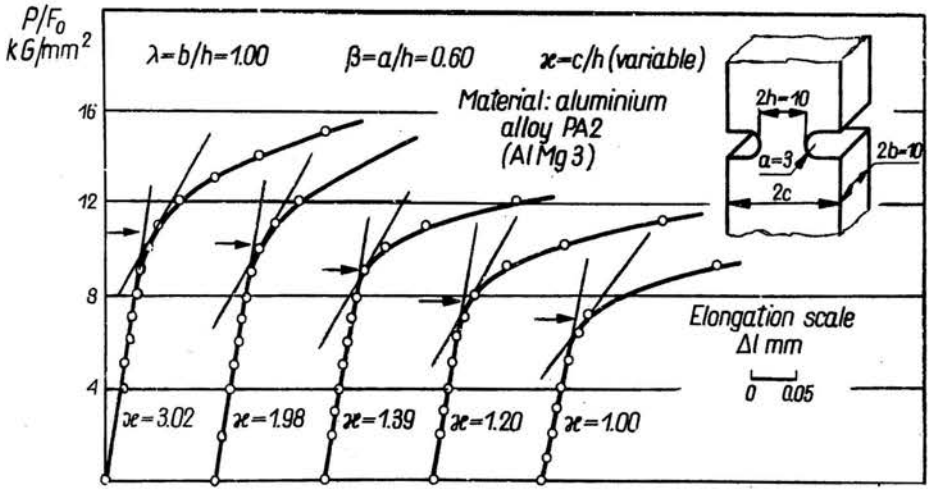

Fig. 10

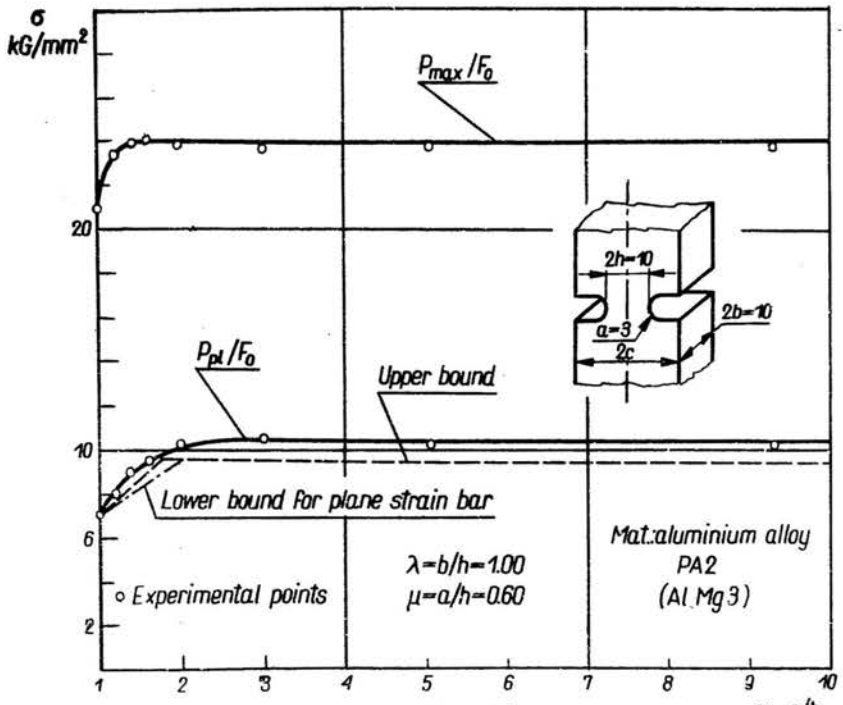

Fig. 11

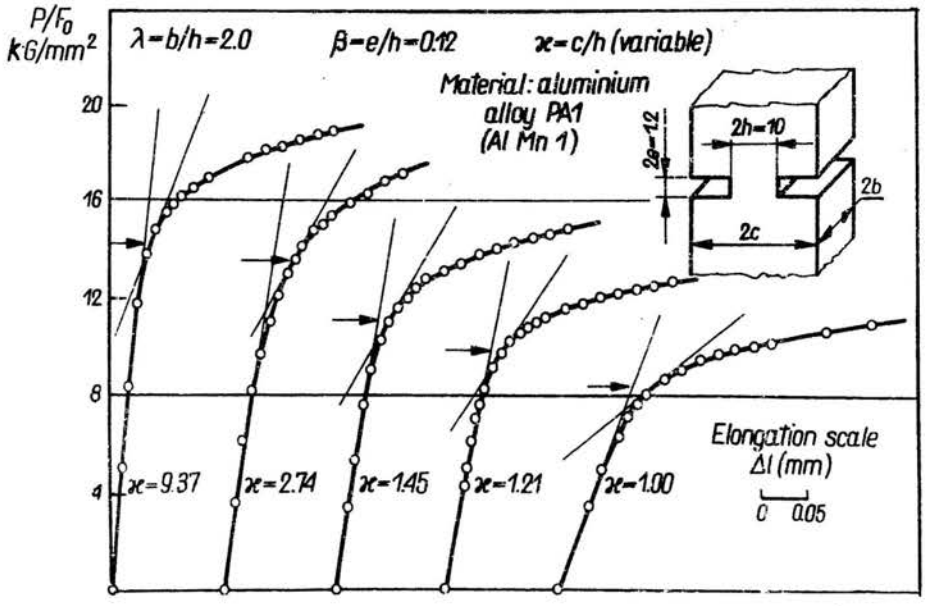

Fig. 12

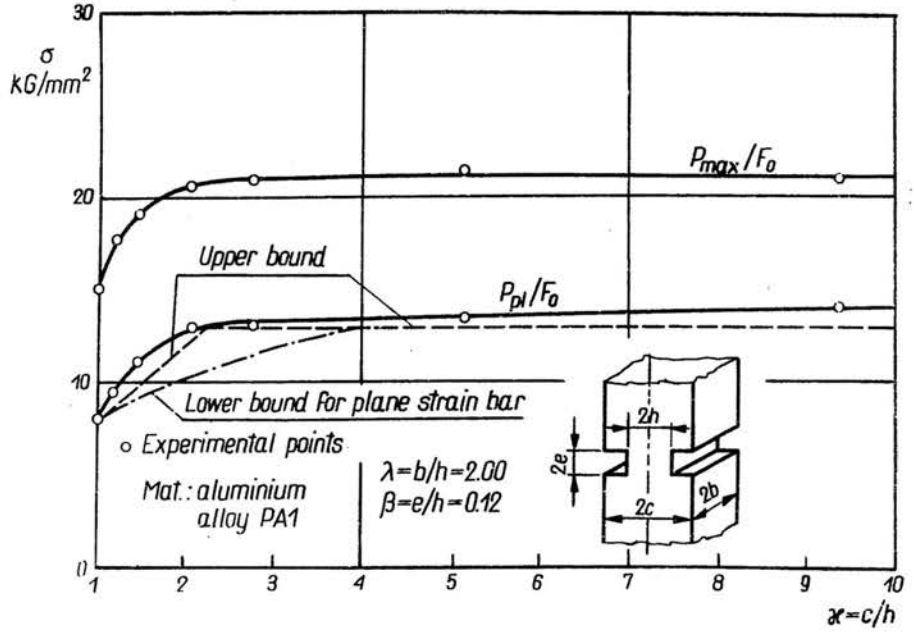

Fig. 13

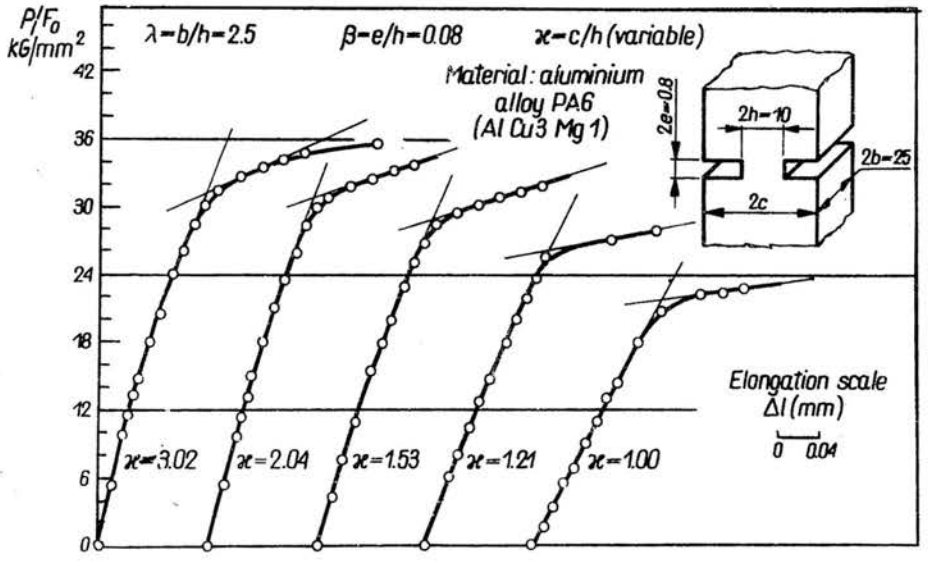

Fig. 14

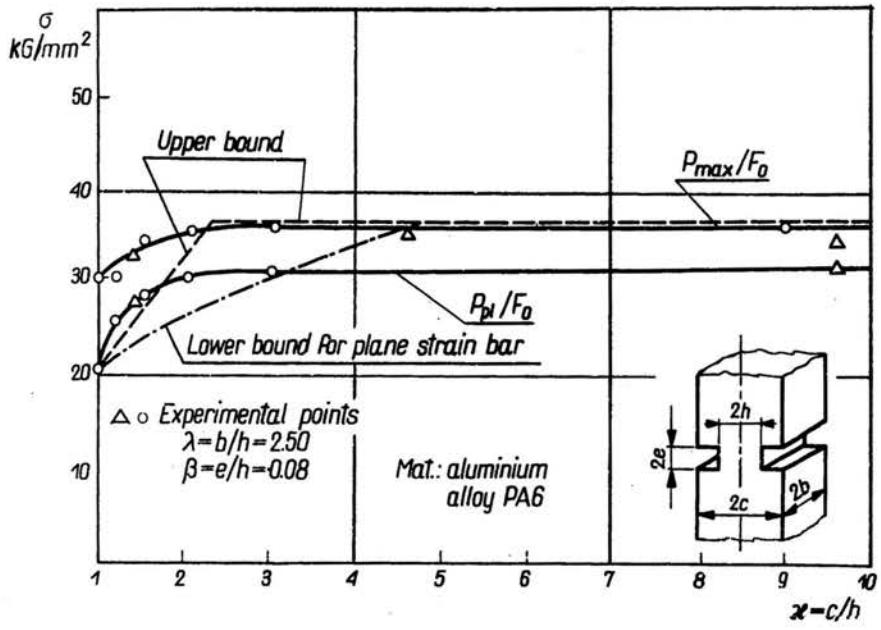

Fig. 15

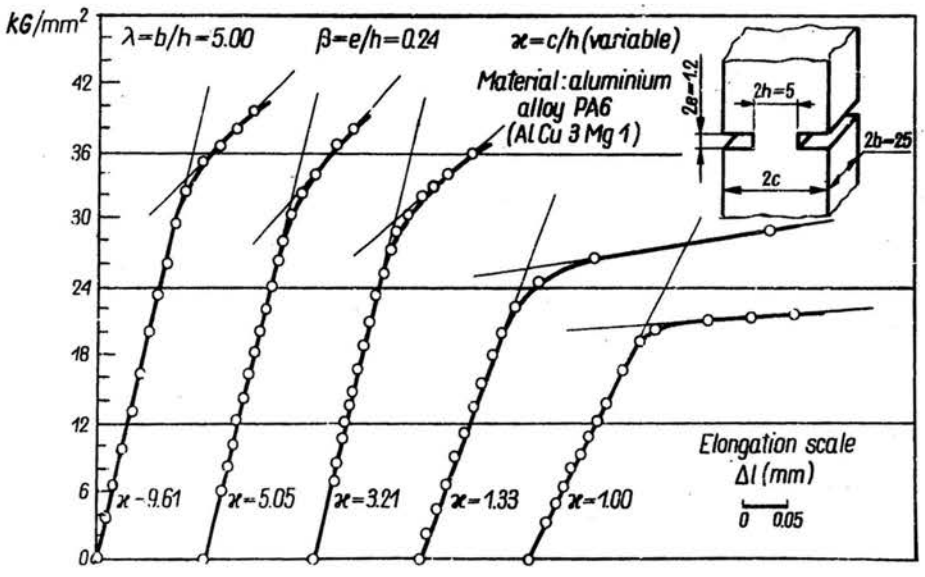

Fig. 16

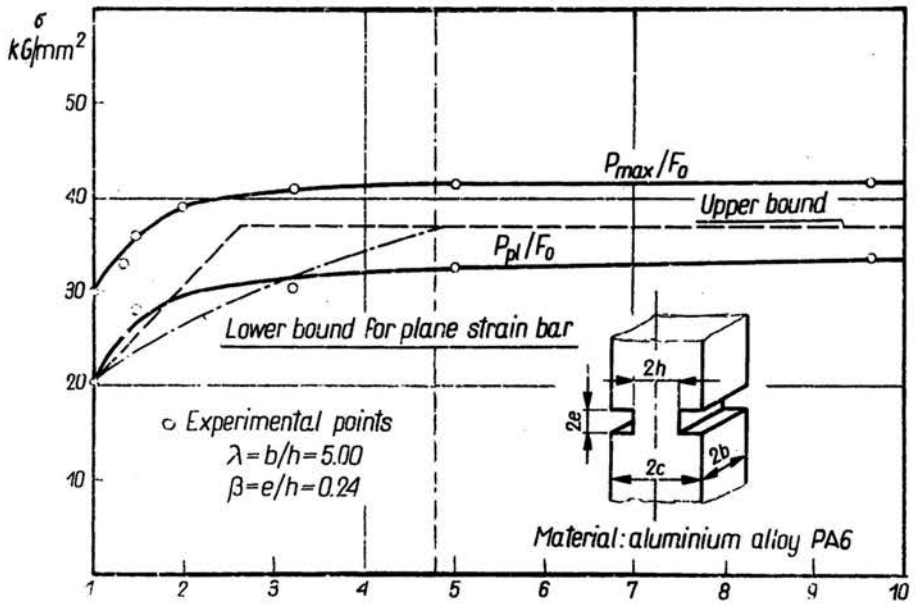

Fig. 17